Iterative migration of gravity and gravity gradiometry data

Le Wan and Michael S. Zhdanov, University of Utah and TechnoImaging*

Summary

The geological interpretation of gravity and gravity gradiometry data is a very challenging problem. 3D inversion represents the only practical tool for the quantitative interpretation of gravity gradiometry data. However, 3D inversion is a complicated and time-consuming procedure that is very dependent on the a priori model and constraints used. 3D migration gives a rapid imaging of a geological target that can be used for interpretation or as an a priori model for subsequent 3D regularized inversion. This method is based on a direct integral transformation of the observed gravity gradients into a subsurface density distribution. Moreover, migration can be applied iteratively to get more accurate subsurface density distribution, and the results are comparable to those obtained from regularized inversion. We present a model study and a case study for the 3D iterative imaging of FTG gravity gradiometry data from Nordkapp Basin, Barents Sea.

Introduction

Density distribution provides important information about subsurface geological formations. Generating 3D density distribution from gravity and/or gravity gradiometry data is a challenging problem. Rigorous 3D inversion of gravity gradiometry data to 3D density models is usually considered as the only practical tool for quantitative interpretation. A number of publications have discussed 3D inversion with smooth (e.g., Li, 2001), and focusing (e.g., Zhdanov et al., 2004) regularization. However, the interpretation workflow for 3D inversion can be complicated and time consuming because it is dependent on a priori models and other geological constraints.

In this paper, we present an alternative approach, one which is based on and extends the idea of potential field migration as originally introduced by Zhdanov (2002). Mathematically, migration is described by an action of the adjoint operator on the observed data. This concept has long been developed for seismic wave fields (e.g., Schneider, 1978; Berkhout, 1980; Claerbout, 1985), and has also been developed for electromagnetic fields (e.g., Wan and Zhdanov, 2005; Zhdanov, 1988, 2002, 2009a, b), where the adjoint operators manifest themselves as the (backward) propagation of seismic or electromagnetic fields in reverse time. When applied to potential fields, migration manifests itself as a special form of downward continuation of the potential field and/or its gradients (Zhdanov et al., 2010, 2011). A downward continuation is applied to the migration field, which is obtained by relocating the sources of the observed field into the upper half-space as mirror images of the true sources. Contrary to conventional downward continuation of the potential field, downward continuation of the migration field is away from the mirror images of the sources. Therefore, migration is a stable transform, similar to upward continuation. At the same time, the migration field does contain remnant information about the original source distribution, which is why it can be used for subsurface imaging. Furthermore, the adjoint operators may be applied iteratively in such a manner that iterative potential field migration is equivalent to regularized inversion. In this paper we develop the principles of the iterative migration. We present a model study and a case study for the 3D iterative imaging of FTG gravity gradiometry data from Nordkapp Basin, Barents Sea.

Gravity gradiometry data

The gravity field, $\mathbf{g}$, is given by the following well known integral formula:

$$\mathbf{g}(\mathbf{r}) = \gamma \iiint_D \rho(\mathbf{r}') \frac{\mathbf{r}'-\mathbf{r}}{|\mathbf{r}'-\mathbf{r}|^3} dv' , \quad (1)$$

where γ is the universal gravitational constant, and ρ is the anomalous density distribution within a domain D.

The second spatial derivatives of the gravity potential $U(\mathbf{r})$,

$$g_{\alpha\beta} = \frac{\partial^2}{\partial\alpha\partial\beta} U(\mathbf{r}) , \quad \alpha,\beta = x,y,z, \quad (2)$$

form a symmetric gravity tensor:

$$\hat{\mathbf{g}} = \begin{bmatrix} g_{xx} & g_{xy} & g_{xz} \\ g_{yx} & g_{yy} & g_{zz} \\ g_{zx} & g_{zy} & g_{zz} \end{bmatrix} . \quad (3)$$

The expressions for the gravity tensor components can be calculated as follows:

$$g_{\alpha\beta=}\gamma \iiint_D \rho(\mathbf{r}') \frac{\mathbf{r}'-\mathbf{r}}{|\mathbf{r}'-\mathbf{r}|^3} K_{\alpha\beta}(\mathbf{r}'-\mathbf{r}) dv' , \quad (4)$$

where the kernels, $K_{\alpha\beta}$, are equal to

$$K_{\alpha\beta}(\mathbf{r}'-\mathbf{r}) = \begin{cases} 3\frac{(\alpha-\alpha')(\beta-\beta')}{|\mathbf{r}'-\mathbf{r}|^2} , & \alpha \neq \beta \\ 3\frac{(\alpha-\alpha')^2}{|\mathbf{r}'-\mathbf{r}|^2} - 1 , & \alpha = \beta \end{cases} \quad (5)$$

Adjoint operators for gravity gradiometry inversion

Let us consider a problem of the inversion of gravity gradiometry data using gradient-type methods. Assume that we have observed some gravity field $g_{\alpha\beta}^{obs}(\mathbf{r})$ on the observational surface S, and the domain D is located in the lower half-space. The problem is to determine the density distribution, $\rho(\mathbf{r}')$. For simplicity, we first ignore the ill-posedness of gravity inversion and reduce the inversion problem to a minimization of the misfit functional between the observed and predicted data:

$$\phi(\rho) = \left\| g_{\alpha\beta} - g_{\alpha\beta}^{obs} \right\|^2 = min . \quad (6)$$

DOI http://dx.doi.org/10.1190/segam2013-1036.1

To solve the minimization problem (6), we can find the direction of steepest ascent at the point ρ of the model space M:

$$l(\rho) = A^*\left(A^g_{\alpha\beta}(\rho) - g^{obs}_{\alpha\beta}\right) = A^*\left(g_{\alpha\beta} - g^{obs}_{\alpha\beta}\right), \quad (7)$$

where the star * denotes the adjoint operator.

The adjoint operator A^* for the gravity gradient problem is equal to (Zhdanov et al., 2011):

$$A^*_{\alpha\beta}(f) = \gamma \iint_S \frac{f(\mathbf{r})}{|\mathbf{r}'-\mathbf{r}|^3} K_{\alpha\beta}(\mathbf{r}'-\mathbf{r})ds\,. \quad (8)$$

Therefore, according to equation (7), the direction of steepest ascent is equal to:

$$l(\rho) = \gamma \iint_S \frac{g_{\alpha\beta}(\mathbf{r}) - g^{obs}_{\alpha\beta}(\mathbf{r})}{|\mathbf{r}'-\mathbf{r}|^3} K_{\alpha\beta}(\mathbf{r}'-\mathbf{r})ds\,, \quad (9)$$

where $g_{\alpha\beta}(\mathbf{r})$ is the predicted gravity gradient field on the observation surface.

Migration of gravity and gravity tensor fields and 3D density imaging

Following Zhdanov (2002) and Zhdanov et al. (2011), the *migration gravity field*, $g^m_\alpha(\mathbf{r})$, is introduced as a result of application of the adjoint gravity operator, A^*_α, to the observed component of the gravity field:

$$g^m_\alpha(\mathbf{r}) = A^*_\alpha g_\alpha\,, \quad (10)$$

In a similar way, we can introduce a *migration gravity tensor field* $g^m_{\alpha\beta}(\mathbf{r})$ and use the following notations for the components of this tensor field:

$$g^m_{\alpha\beta}(\mathbf{r}) = A^*_{\alpha\beta} g_{\alpha\beta} \quad (11)$$

where the adjoint operators, $A^*_{\alpha\beta}$ applied to some function $f(\mathbf{r})$, are given by equations (8).

We should note, however, that the direct migration of the observed gravity and/or gravity tensor fields does not produce an adequate image of the subsurface density distribution because the migration fields rapidly attenuate with the depth. In order to image the sources of the gravity fields at their correct locations, one should apply an appropriate spatial weighting operator to the migration fields. This weighting operator is constructed based on the integrated sensitivity of the data to the density.

$$\rho^m_\alpha(\mathbf{r}) = k_\alpha (W^*_m W_m)^{-1} A^*_\alpha g_\alpha = k_\alpha w^{-2}_\alpha(z) g^m_\alpha(\mathbf{r})\,, \quad (12)$$

where unknown coefficient k_α can be determined by a linear line search and the linear weighting operator W_m is equal to the square root of the integrated sensitivity of the gravity field (Zhdanov, et al, 2011).

In a similar way, we can introduce a migration density based on the gravity tensor migration:

$$\rho^m_{\alpha\beta}(\mathbf{r}) = k_{\alpha\beta} (W^*_m W_m)^{-1} A^*_{\alpha\beta} g_{\alpha\beta} = k_{\alpha\beta} w^{-2}_{\alpha\beta}(z) g^m_{\alpha\beta}(\mathbf{r}) \quad (13)$$

where $k_{\alpha\beta}$ can be determined by a linear line search and the linear weighting operator W_m is equal to the square root of the integrated sensitivity of the gravity field (Zhdanov, et al, 2011).

Equation (12) is called a migration density, $\rho^m_\alpha(\mathbf{r})$ and expression (13) is called a *tensor field migration density*. It is proportional to the magnitude of the weighted migration field, $g^m_\alpha(\mathbf{r})$ or tensor migration field $g^m_{\alpha\beta}(\mathbf{r})$. Thus, migration transformation provides a stable algorithm for calculating migration density.

Iterative migration

Equations (12) and (13) produce a migration image of the density distribution in the lower half-space. However, a better quality migration image can be produced by repeating the migration process iteratively. We begin with the migration of the observed gravity and/or gravity tensor field data and obtaining the density distribution by migration imaging. In order to evaluate the accuracy of our migration imaging, we apply a forward modeling operator and compute a residual between the observed and predicted data for the given density model. If the residual is smaller than the prescribed accuracy level, we use the migration image as a final density model. In the case where the residual is not small enough, we apply the migration to the residual field and produce the density variation, $\delta\rho_1$, to the original density model using the same transformation, as we have applied to the original migration field:

$$\rho_2 = \rho_1 + \delta\rho_1 = \rho_1 - k_1 (W^*_m W_m)^{-1} l_1\,, \quad (14)$$

where l_1 stands for the migration image obtained by residual field migration, equation (7).

A general scheme of the iterative migration can be described by the following formula:

$$\rho_{n+1} = \rho_n + \delta\rho_n = \rho_n - k_n (W^*_m W_m)^{-1} l_n\,, \quad (15)$$

The iterative migration is terminated when the residual field becomes smaller than the required accuracy level of the data fitting.

Similar to iterative inversion, iterative migration can be implemented with regularization (Zhdanov, 2002). This also allows us to apply both the smooth and focusing stabilizers. In this case, equation (15) can be re-written as follows:

$$\rho_{n+1} = \rho_n + \delta\rho_n = \rho_n - k_n (W^*_m W_m)^{-1} l^\lambda_n\,, \quad (16)$$
$$l^\lambda_n = l_n + \lambda\left(\rho_n - \rho_{apr}\right),$$

where λ is the regularization parameter; l_n is a gradient direction on the *n*-th iteration, computed using formulas (9), and l^λ_n is the regularized gradient direction on the *n*-th iteration.

Model study

We have examined the effectiveness of the iterative migration using synthetic gravity and gravity gradiometry data computed for a simple model, shown in Figure 1. For testing the algorithm, the "observed data" generated for this

DOI http://dx.doi.org/10.1190/segam2013-1036.1

model were contaminated by 5% random noise. The model consists of two rectangular bodies with sides of 450m, 550m, and 450m in the x, y and z directions, respectively. The top surface of one body is at a depth of 150 m, while the top surface of another body is at a depth of 250 m below the ground surface. Both bodies have a density of 1 g/cm^3. Figure 1 shows the plane view and a vertical section across the bodies. The observation surface is 30 m above the ground. The area of observation extends from -1150 m to 1150 m in the x direction and from -750 m to 750 m along the y direction, with a 25 m interval between the data points. There are 93 x 61 = 5673 data points for each component of the gravity field and gravity gradiometry tensor.

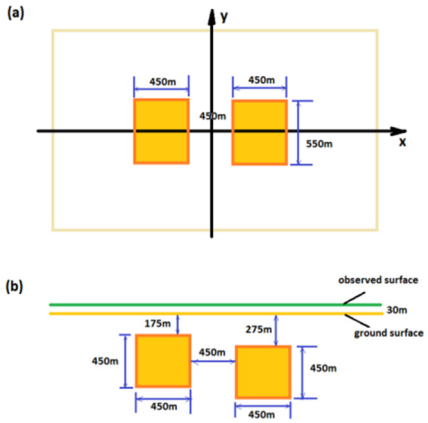

Figure 1 A model of two rectangular bodies with a density of 1 g/cm3. Panel (a): a plane view of the model; panel (b): a vertical cross section of the model.

Figure 2 shows a comparison of the observed and predicted data for g_{zz} component at profile $y = 0$ m computed based on the migration images of the density distribution. The solid blue line shows the observed field; the dashed red line presents the field computed from the density model obtained by migration only; the dotted green line and the dotted purple line show the fields computed from the density model obtained by iterative migration with smooth and focusing stabilizers, respectively. One can see that even for the noisy observed data, results obtained with both smooth and focusing stabilizers produce the predicted data that fit the observed data well.

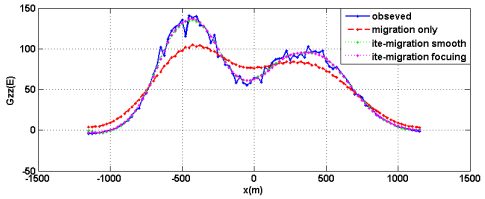

Figure 2 Comparison of the observed and predicted data for the g_{zz} component at profile $y = 0$ m computed based on the migration images of the density distribution.

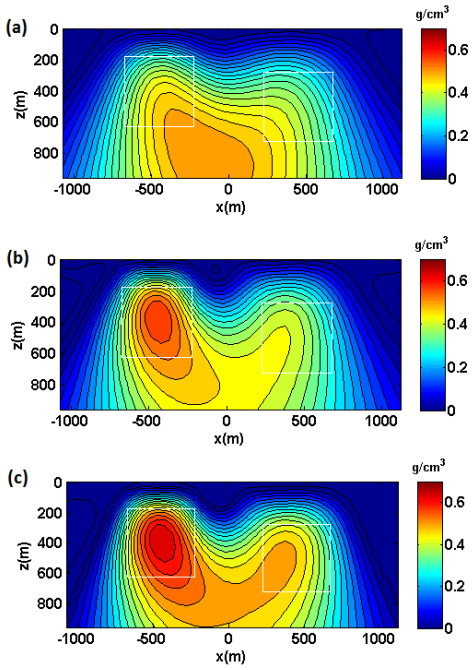

Figure 3 Vertical sections of the density models obtained by migration only (panel a); by iterative migration with smooth stabilizer (panel b) and by iterative migration with focusing stabilizer (panel c) of g_{zz} component.

Figure 3 presents vertical sections of the density models obtained by migration only (panel a); by iterative migration with the smooth stabilizer (panel b) and by iterative migration with the focusing stabilizer (panel c) of g_{zz} component. All data fitting is within 5%, which is the noise level. The solid white line shows the true model location. One can see that the iterative migration shows a better image of the true model than one time migration, and the iterative migration with the focusing stabilizer produces the best image.

Case study: Migration of FTG data at the Nordkapp Basin

The Nordkapp basin is a deep, narrow salt basin in the southern Barents Sea. The southwestern part of the Nordkapp Basin (Obelix survey location) is a narrow, northeast-trending sub-basin 150 km long and 25-50 km wide. It contains some 17 salt diapirs located along the basin's axis (Figure 4). The northeastern part is a wider East-trending sub-basin about 200 km long and 50-70 km wide. More than 16 salt diapirs occur west of the 32° E meridian. The goal of the FTG survey was to provide additional information for evaluation of these complex salt overhang geometries. The targets of this study were the salt diapirs G2 and F2 (see Figure 5). A typical density of the base tertiary rocks in the area of investigation is within 2.30-2.38 g/cm^3.

DOI http://dx.doi.org/10.1190/segam2013-1036.1

Salt diapirs are characterized usually by negative density anomalies.

The maps of the g_{zz} component of the full tensor gradiometry (FTG) data are given in Figure 5.

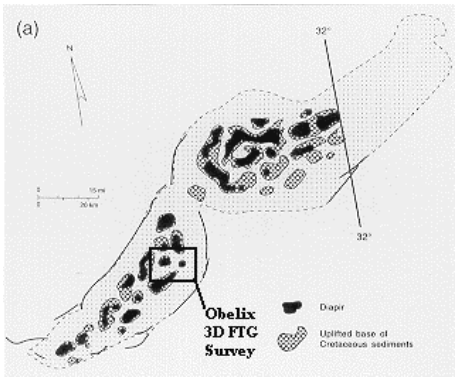

Figure 4 Simplified structural map of the Nordkapp Basin showing salt diapirs and main fault zones. Black = sub-crop of diapirs at or near Pliocene-Pleistocene unconformity.

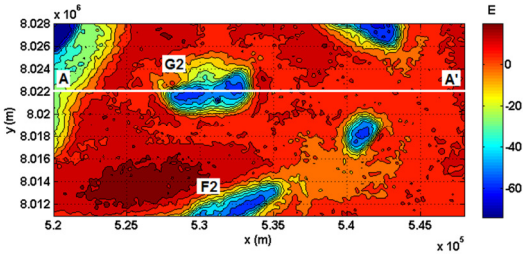

Figure 5 Maps of the g_{zz} component of the full tensor gradiometry (FTG). The white line shows the location of the A-A' profiles.

We ran the migration for the g_{zz} component of the gravity tensor. We have selected a modeling domain 28 km (east-west) x 17 km (north-south) and extended at a depth of 6 km. This volume of migration was discretized in 281 x 171 x 59=2,835,009 cells; the cell size is 100 m x 100 m x 100 m. Thus, the selected modeling domain may represent a salt base or a deeper source down to approximately 6 km for salt structures G2 and F2. All iterative migrations were run until the misfit between the predicted and observed data reached 5%.

Figure 6 shows a vertical section of the iterative migration result along the profile A-A'. The upper panel in Figure 6 shows the observed data (solid blue line) vs predicted data (dashed red line), while the lower panel shows the density image along the A-A' profile, obtained by iterative migration. For comparison, we present in Figures 7 the 3D inversion results for the same data from Wan and Zhdanov, 2008. One can see that the migration and inversion results are almost the same. One can clearly see the salt diapir G2 in these images.

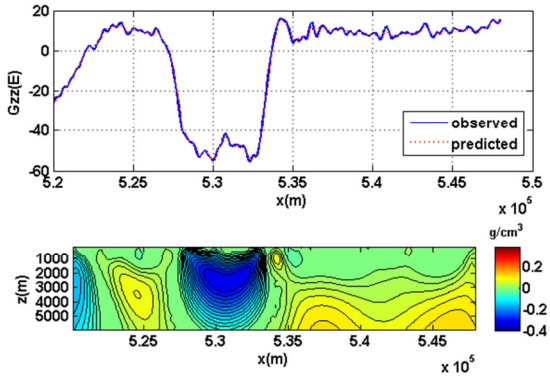

Figure 6 Top panel: observed and predicted data for the migration result. Bottom panel: a vertical section of 3D iterative migration result for the g_{zz} component along the A-A' profile.

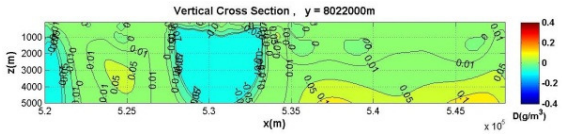

Figure 7 A vertical section of the 3D inversion result for the g_{zz} component along the A-A' profile.

Conclusion

Potential field migration is a direct integral transformation of the gravity field and /or gradients into 3D density distributions. Iterative migration is practically equivalent to the basic inversion algorithm with one very important difference: the density perturbation at each iteration is determined by migration transformation of the corresponding gravity or gravity gradient residual field data, which is similar to upward continuation. This is significant because the last transformation is very well developed in the theory of the potential field interpretation. In other words, the iterative migration makes it possible to use the powerful and stable technique of upward continuation for the solution of the inverse problem.

As demonstrated with our Nordkapp Basin FTG case studies, the results of 3D potential field iterative migration are similar to those obtained from 3D regularized inversion.

Acknowledgments

The authors acknowledge the support of the University of Utah Consortium for Electromagnetic Modeling and Inversion (CEMI) and TechnoImaging.

We are thankful to Dr. Brian Farrelly for providing the gravity gradiometer data and for permission to publish the results.

DOI http://dx.doi.org/10.1190/segam2013-1036.1

http://dx.doi.org/10.1190/segam2013-1036.1

EDITED REFERENCES

Note: This reference list is a copy-edited version of the reference list submitted by the author. Reference lists for the 2013 SEG Technical Program Expanded Abstracts have been copy edited so that references provided with the online metadata for each paper will achieve a high degree of linking to cited sources that appear on the Web.

REFERENCES

Berkhout, A. J., 1980, Seismic migration: Elsevier.

Claerbout, J. F., 1985, Imaging the earth's interior: Blackwell Scientific Publications.

Li, Y., 2001, 3D inversion of gravity gradiometer data: 71st Annual International Meeting, SEG, Expanded Abstracts, doi: 10.1190/ 1.1816383.

Schneider, W.,A., 1978, Integral formulation for migration in two and three dimensions: Geophysics, **43**, 49–76, http://dx.doi.org/10.1190/1.1440828.

Wan, L., and M. S. Zhdanov, 2005, Rapid seabed imaging by frequency domain electromagnetic migration: Presented at the 75th Annual International Meeting, SEG.

Wan, L., and M. S. Zhdanov, 2008, Focusing inversion of marine full-tensor gradiometry data in offshore geophysical exploration: 78th Annual International Meeting, SEG, Expanded Abstracts, 751–754.

Zhdanov, M. S., 1988, Integral transforms in geophysics: Springer-Verlag.

Zhdanov, M. S., 2002, Geophysical inverse theory and regularization problems: Elsevier.

Zhdanov, M. S., 2009a. Geophysical electromagnetic theory and methods: Elsevier.

Zhdanov, M. S., 2009b, New advances in 3D regularized inversion of gravity and electromagnetic data: Geophysical Prospecting, **57**, 463–478, http://dx.doi.org/10.1111/j.1365-2478.2008.00763.x.

Zhdanov, M. S., R. G. Ellis, and S. Mukherjee, 2004, Regularized focusing inversion of 3D gravity tensor data: Geophysics, **69**, 925–937, http://dx.doi.org/10.1190/1.1778236.

Zhdanov, M. S., X. Liu, and G. Wilson, 2010, Potential field migration for rapid 3D imaging of entire gravity gradiometry surveys: First Break, **28**, 47–51.

Zhdanov, M. S., X. Liu, G. Wilson, and L. Wan, 2011, Potential field migration for rapid imaging of gravity gradiometry data: Geophysical Prospecting, **59**, 1052–1071.